The Effects of Remodeling with Heart Failure on Mode of Initiation of Ventricular Fibrillation and its Spatiotemporal Organization

Thomas H. Everett, IV, PhD[1], George S. Hulley, MD[2], Ken W. Lee, MD[2],

Roger Chang, BS[2], Emily E. Wilson, BS[2], Jeffrey E. Olgin, MD[2]

[1] Krannert Institute of Cardiology, Indiana University School of Medicine,

[2] Division of Cardiology and the Cardiovascular Research Institute
University of California San Francisco

Running Title: Spatiotemporal Organization of VF

Word count: 5168 words

Correspondence to
Thomas H. Everett, IV, PhD
Krannert Institute of Cardiology
1800 N. Capitol, Ste. E400E
Indianapolis, IN 46202
(317)672-2190
theveret@iu.edu

Funding Sources

NIH grant RO1-HL072854 (JEO), RC1 HL099789 (JEO & THE) and AHA Western States Affiliate Beginning Grant-in-Aid 0765177Y (THE)

Conflict of Interest Disclosures:

Thomas Everett – None
George Hulley - None
Ken Lee – None
Roger Chang - None
Emily Wilson – None
Jeffrey Olgin - None

This is the author's manuscript of the article published in final edited form as:

Everett, T. H. 4th, Hulley, G. S., Lee, K. W., Chang, R., Wilson, E. E., & Olgin, J. E. (2015). The effects of remodeling with heart failure on mode of initiation of ventricular fibrillation and its spatiotemporal organization. Journal of Interventional Cardiac Electrophysiology, 43(3), 205–215. http://doi.org/10.1007/s10840-015-0016-2

Abstract

Introduction - The effect of the heart failure substrate on the initiation of ventricular fibrillation (VF), and its resulting mechanism is not known. The objective of this study was to determine the effects of substrate on VF initiation and its spatiotemporal organization in the heart failure model.

Methods - Optical action potentials were recorded from LV wedge preparations from either structurally normal hearts (control, n=11) or from congestive heart failure (CHF, n=7), at the epicardial surface, endocardial surface which included a papillary muscle, and a transmural cross section. Action potential duration (APD_{80}) was determined, and VF was initiated. A fast Fourier-transform was calculated, and the dominant frequency (DF) was determined.

Results - The CHF group showed increased VF vulnerability (69% vs 26%, $p<0.03$), and every mapped surface showed an APD_{80} gradient which included islands of higher APDs on the transmural surface (M-cells) which was not observed in controls. VF in the CHF group was characterized by stable, discrete high DF areas that correlated to either foci or spiral waves located on the transmural surface at the site of the papillary muscle. Overall the top 10% of DFs correlated to an APD of 101 ms while the bottom 10% of DFs correlated to an APD of 126 ms ($p<0.01$).

Conclusion - In the CHF model, APD gradients correlated with an increased vulnerability to VF, and the highest stable DFs were located on the transmural surface which was not seen in Controls. This indicates that the CHF substrate creates unique APD and DF characteristics.

Key Words

Ventricular fibrillation, Fourier analysis, alternans, mapping, heart failure

Abbreviations

APD – action potential duration

BCL – basic cycle length

CHF – congestive heart failure

DF – dominant frequency

VF – ventricular fibrillation

Introduction

In the presence of heart failure, structural and electrical remodeling occurs that begins at the cellular level with changes in cell size, the distribution of connexins, ion channels, and an increase in fibrosis levels.[1] This remodeling of the myocardium creates a substrate that leads itself to prolonged action potential duration (APD), an increased dispersion of refractoriness, APD alternans, and conduction disturbances that can lead to an increase in arrhythmogenecity and ventricular fibrillation (VF).[2, 3]

APD gradients have been demonstrated on the LV epicardial surface,[4, 5] and within the transmural myocardium which includes a subpopulation of cells with longer APDs that have been referred to as M-cells.[6-8] However, the debate continues as to whether M-cells exist, where they are located, and their significance in the electrophysiological properties of the ventricle.[9] Finally, the papillary muscle has also been shown to play a role in VF initiation and maintenance.[10, 11] However, most of these studies have been performed in structurally normal hearts, and which plays more of a role in VF vulnerability (activation or repolarization remodeling), and how it effects the resulting VF in the heart failure model is still poorly understood.

The purpose of this study was to investigate the electrophysiological characteristics of the different surfaces of the LV in the heart failure model with optical mapping and to assess the contributing factors to the vulnerability to VF. Finally, this study also compared the spatiotemporal organization of VF within the heart failure substrate to that of structurally normal hearts, with the hypothesis that VF in the setting of heart failure would have different characteristics than that of structurally normal hearts.

Methods

An expanded Methods section is available in the Data Supplement. All animal protocols were reviewed and approved by the University of California San Francisco Laboratory Animal Resource Center's Institutional Animal Care and Use Committee, conformed to the regulations for humane care and treatment of animals established by the National Institute of Health, and were conducted with the assistance/supervision of the Animal Resource Department veterinary staff.

Eighteen dogs weighing 25-30 Kg were divided into two groups: control (n=11), and pacing-induced congestive heart failure (CHF) (n=7).

Animal Models

Heart Failure (CHF) was induced in 7 dogs via four weeks of rapid ventricular pacing at 240 bpm with ablation of the AV node .[12] Ventricular function was monitored weekly with transthoracic echocardiography.

Optical Mapping Studies

A left ventricular wedge preparation (Data Supplement Figure 1) was used in an optical mapping system that has been previously described.[13] PGH-1 was used to map membrane potentials during pacing and VF.[14] The APD at 80% repolarization (APD_{80}) was determined, and APD_{80} alternans were quantified. Activation patterns and wave-front direction during VF were determined from raw fluorescence movies (isopotential).

The optical mapping recordings were sampled at 2,000 Hz, and for each signal the dominant frequency (DF) was determined as described previously.[15] Ventricular tissues were then saved for histological analysis of fibrosis.[16]

Statistical Analysis

Data were summarized with means and standard deviations for continuous measures. Tabulations and percentages were used to summarize categorical variables. The associations of the FFT, APD, and conduction velocity outcomes with recording site, surface, and group were analyzed using linear mixed effects models. The mixed effects models employed random dog effects to account for the statistical dependence among multiple measures within the same dog, both within and across recording locations. A generalized mixed effect model was also used for APD alternans and VF vulnerability. Statistical significance was defined as at the level of 0.05. All analyses were conducted in SAS Version 9.2 (SAS Institute Inc., Cary, NC).

Results

Summary conduction velocity and conduction heterogeneity results between models are shown in Figure 1. Results between surfaces within each model are shown in Data Supplement Figure 2. In the Control group, the epicardial surface had significantly faster conduction velocity values and lower heterogeneity measurements than the other surfaces. The Control epicardial surface also had significantly faster conduction velocity values than those in the CHF group. The CHF group had similar conduction velocity values for all mapped surfaces, and the transmural surface had similar values for both models. As shown in Figure 2A, the APD_{80} data shows longer values on the transmural surface of both groups. This difference reached significance in the Control group. There were no significant differences in fibrosis levels between Control and CHF groups for all mapped surfaces.

APD Gradients

Every mapped surface in the CHF group showed an APD gradient while this result was seen in only 2 mapped Control surfaces from the same wedge preparation. Data Supplement Figure 3 shows examples of gradients that were seen in the CHF group, and Data Supplement

Figure 4 shows an example from the Control group. Each figure also has examples of signals from the areas of the longest and shortest APD_{80} within the field of view. The example of the CHF epicardial surface, shows a gradient with longer APDs towards the base and shorter APDs towards the apex. For the endocardium example, the gradient was characterized by long APDs at the base of the papillary muscle and shorter towards the top of the muscle. All of the mapped CHF transmural surfaces had the highest measured APD_{80} in the middle of the field of view, with decreasing APDs toward the endocardial and epicardial surfaces. An example of this type of APD_{80} distribution is shown in Figure 2C with example optical action potentials. The results of the calculated APD_{80} gradient for each surface of the CHF model are shown in Figure 2B.

Summary APD_{80} variability is shown in Figure 2A as the difference between the 95^{th} and 5^{th} percentiles. With APD_{80} gradients in the CHF group described above, a wide spread between the 95^{th} and 5^{th} percentiles is seen. Even though an APD_{80} gradient is not seen in the Control group, there is still a large amount of variability in the APD_{80} values on the endocardium and transmural surfaces.

APD Alternans

Every CHF preparation had at least one mapped surface that exhibited alternans. While only one Control dog showed evidence of alternans that occurred on the endocardial and transmural surfaces (Figure 3). As Figure 3 shows, the CHF group had a higher frequency of APD alternans than the Control group on the epicardial and transmural surfaces. An example signal from a CHF transmural surface during pacing at 300 ms is shown in figure 3B.

VF Inducibility

Figure 3C shows the percentage of VF that was induced with an extra stimulus from each pacing site for each mapped surface. As the figure shows, the CHF group had a higher incidence

of induced VF compared to controls. The type of activation that initiated VF fell into several categories.

For the CHF group, (1) an area of block expands as the S1/S2 coupling shortens causing unidirectional block of the extra stimulus, initiating reentry within the field of view; (2) unidirectional block of the extra stimulus is observed, however the mechanism of VF initiation is outside the field of view; (3) unidirectional block is not observed within the field of view, and both the S1 and S2 have similar conduction characteristics, but VF is still initiated. For the Control group, (1) area of block develops as S1/S2 coupling shortens initiating reentry; or (2) similar to (3) in the CHF group, unidirectional block is not observed, but VF is still initiated.

Figure 4 shows examples of activation maps in which VF was initiated with an extra stimulus. In these examples, an increased amount of conduction slowing was seen with a closely coupled extra stimulus. In the Control group, this occurred with closer coupled intervals than in the CHF group.

When VF inducibility was compared to conduction velocity and conduction heterogeneity through phase metrics (p50, and p95-5), the CHF group showed no correlation between conduction anisotropy and VF inducibility (Figure 5). The Control group did show a significant difference in the p50 and p95-p5 metrics only on the epicardial surface.

VF inducibility was then compared to the distribution of APDs. As Figure 6 shows, the CHF group had a significant difference between the variability of APDs in which VF was initiated as compared to no VF initiation only on the transmural surface. In contrast, the Control group had significantly higher APD variability in which VF was induced on both the epicardial and endocardial surfaces, but not on the transmural surface.

VF Characteristics

Table 1 shows the types of activation patterns that were seen on each mapped surface for each dog along with the location of the stable, discrete high DF areas. Figure 7 shows a conduction map of each type of ventricular fibrillation mechanism that was observed. As the table shows, 6 of 7 CHF dogs had at least one surface with a stable, high DF area including all of the mapped transmural surfaces. In comparison, only 3 of the 11 Controls had at least one surface with VF that was characterized by high DF areas. Figure 8 shows examples of DF maps for each of the surfaces of each group. The CHF example shows a high DF area on the transmural surface that contained higher DFs than what were seen on the other surfaces.

Epicardial Surface

For the Control group, only 2 of the 10 mapped epicardial surfaces showed evidence of focal activation. These two surfaces also corresponded to having stable, high DF areas. All others had activation patterns of either multiple wavelets or one broad wavefront dominating the field of view. Similar results were seen in the CHF group, which had 2 of 6 mapped surfaces with either focal activation or a spiral wave. These types of activation corresponded to stable, high DF areas. All other dogs had either multiple wavefronts or one broad wavefront dominating the field of view. These activation patterns had either transient DFs (multiple wavefronts) or the area was dominated by one DF (broad wavefront).

Endocardial Surface

Mapping of the endocardial surface included the papillary muscle and only the CHF group had VF characterized by stable, high DF areas that correlated to spiral waves or focal activation patterns. Even though 2 of 7 endocardial surfaces in the Control group had activation characterized by spiral waves, no discrete, stable DFs were observed. The others had either multiple or broad wavefront activation.

Transmural Surface

The transmural surface had the highest percentage of spiral wave and focal activation when compared to the other mapped surfaces. In the CHF group, the transmural surface had VF activation patterns of either a spiral wave or focal activation, and the VF was characterized by stable, discrete, high DF areas. An example of an intramyocardial spiral wave from this group is shown in the Data Supplement along with its corresponding DF map in Data Supplement figure 5. In the Control group, 75% of the transmural surfaces had focal activation. Only one of these did not correlate to stable, high DF areas.

Dominant Frequencies

As Figure 8 shows, the CHF endocardial and transmural surfaces showed a significant correlation between APDs and DFs during VF. This inverse relationship shows that high DFs are correlated to shorter APDs and vice versa. Even though the summary data for the epicardial surface shows no correlation, the correlation still exists when each individual dog is analyzed (Figure 8C). DF maps are shown along with the APD maps in the data supplement to demonstrate this correlation that only occurred in the CHF group. The examples from the Control group in Data Supplement Figure 4 show how this relationship did not apply to this group.

Discussion

This study has shown that the electrical remodeling that occurs in heart failure alters the APD characteristics of the tissue. In the CHF group, APD gradients were seen on every surface

with the gradient on the transmural surface characterized by M-cells. This group also had increased VF vulnerability compared to Controls, which was correlated to APD variability and APD alternans, and not to conduction velocity or conduction anisotropy. In most of the Control preparations, VF had to be initiated with burst pace stimulation, indicating that the threshold for VF inducibility was higher than that of the CHF preparations. Several studies have investigated activation or repolarization remodeling that occurs with heart failure, showing that each could influence arrhythmia initiation and VF vulnerability.[3] This study has shown that repolarization remodeling plays the key role in VF vulnerability in the CHF substrate.

This study also demonstrated that the substrate in which the VF occurs plays a role in its resulting mechanism. The CHF group had VF characterized by discrete, stable high-DF areas which correlated to mechanisms of either a spiral wave or focal activation. This included all of the transmural surfaces in the CHF group. Also, it was shown that the distribution of DFs correlated to the APD. In contrast, the control group had a lower percentage of VF characterized by high-DF areas and more VF patterns of multiple wavefronts or one broad wavefront. In addition, no APD/DF correlation was observed. The structural remodeling that occurs with CHF may promote the stability of VF drivers that are characterized by stable, high-DF areas.

M-cells and APD Heterogeneity

Several studies have shown transmural repolarization heterogeneities exist creating an electrical substrate for arrhythmias.[6-8] Contributing to the heterogeneity of repolarization, islands of cells within the mid-myocardium have been identified as having longer APDs than the surrounding cells. Even though these heterogeneities in repolarization have been well described in isolated myocardial cells,[17] thin slices of myocardium,[18] and ventricular wedge preparations,[8] controversy still exists with regard to whether these islands of cells only occur in isolated

preparations, and if they do occur is it only in certain locations of the myocardium.[19] In the current study, in the heart failure substrate, we have shown the existence of a grouping of cells in the mid intramyocardium at the papillary muscle that has longer APDs than the rest of the transmural area. This supports what has previously been shown in canine LV wedge preparations.[6, 8]

It has also been shown that there exists a transepicardial gradient which has been demonstrated to influence VF dynamics.[4] Optical mapping of guinea pig hearts has shown an apex-base APD gradient,[4, 5] which was also shown in pigs *in situ*.[20] However contrary to those studies, an APD gradient could not be observed in a whole rabbit heart,[21] and cells isolated from the LV of rabbit hearts from the apex had longer APDs than cells from the base.[22] The present study has shown that there exists an APD distribution gradient on the epicardial surface in the CHF group. However, a consistent APD gradient was not seen in the Control group.

APD Alternans

T-wave alternans (TWA) have been shown to be prevalent in patients with heart disease, and thus have been considered to be a predictor of sudden cardiac death. Underlying TWA at the cellular and tissue levels are repolarization alternans[23]. The mechanism of alternans has been linked to abnormalities in intracellular calcium cycling, APD restitution, and mechanoelectrical feedback[24]. The remodeling of ion channels and the loss of normal cellular calcium cycling associated with heart failure, can lead to a greater susceptibility to repolarization alternans and arrhythmias. Optical mapping of canine heart failure LV wedge preparations showed that there was an increased incidence of repolarization alternans that was associated with impaired calcium handling which correlated with an increase in VF vulnerability.[25] Similarly, in the present study, the CHF group had a higher incidence of APD alternans and also increased VF vulnerability.

Mechanisms of VF

A majority of the research performed studying the mechanisms of VF have been on either the epicardial or endocardial surface in structurally normal hearts rather than under a pathological condition predisposing to VF. In mapping studies specifically involving the papillary muscle, it has been demonstrated that the RV papillary muscle helps to initiate reentry by serving as a site for wave break,[10] and for anchoring of reentrant wavefronts. The papillary muscle has also been shown to be the site of the highest DF during VF. Subsequent ablation significantly reduced VF inducibility.[11] For studies with diseased hearts, it has been shown that VF in the setting of heart failure has lower DFs, a lower peak dV/dt, a slower activation rate, a significantly lower occurrence of reentry, and an increased occurrence of block than that of VF in controls[26, 27]. We have previously shown with non-contact mapping that in the setting of heart failure, either a focal driver or a stable reentrant rotor can occur[12], while in the Control group, reentrant rotors meander around the posterior LV. In the present study, stable spiral waves or focal activation were seen in the CHF dogs that correlated to stable, high DF areas. These occurred at the transmural surface at the site of the papillary muscle. In the Control group, the majority of the VF activation patterns consisted of multiple wavefronts or one broad wavefront dominating the field of view.

Intramural Reentry

Reentry has been commonly seen during VF with optical mapping on either the epicardial or endocardial surfaces[27], and data from the present study supports these findings. However, few studies have investigated reentry in the intramural myocardium. It has been shown to be theoretically possible for three-dimensional reentry to occur[28], and studies have

provided evidence that three-dimensional scroll waves do occur[22], however they occurred early in the VF[29] and have been short-lived.[30] In the Control group in this study, we did not observe any stable spiral waves and only observed focal activation. Intramyocardial spiral waves were only in the heart failure group in which stable reentry was observed. It is not known if this reentry was responsible for sustaining the VF, however the DF maps that correlated to spiral waves on the transmural surface had higher DFs then what was seen on the other surfaces.

Limitations

This study was performed in canine hearts, and it is not known if human cardiac tissue would respond in a similar manner. However, transmural APD characteristics in failing human hearts have been shown to be greatly reduced compared to controls and mid-myocardial areas of longer APDs were only observed in a percentage of non-failing hearts.[31] The present study was performed with LV wedge preparations, which has been shown to differ from whole heart preparations.[32] In addition, contractility was blocked with 15 mM 2,3-butadione monoxime (BDM; Sigma-Aldrich) which has been shown to affect the APD and conduction velocity. [33, 34] However, the same protocol was applied to all left ventricular wedge preparations, and the APDs were consistently stable throughout the protocol. In addition, there was no difference in dye uptake (or signal amplitude) in the areas with lower APDs. Due to the limitations of optical mapping using a photodiode array, the entirety of the LV was not mapped, and not all surfaces were mapped simultaneously. Therefore, it is not known if the high-frequency areas seen are driving the VF. In addition the three-dimensional characteristics of the M-cells cannot be determined.

Conclusion

APD gradients were observed in the CHF models that were not seen in Control. These gradients also included M-cells which only existed in the CHF model with straight pacing, and correlated to a significant increase in VF vulnerability. This increased VF inducibility was not related to conduction anisotropy in the CHF model, but APD characteristics proved to be more of a factor as APD gradients could influence the vulnerability to arrhythmias. During VF, the CHF model showed mechanisms of either stable spiral waves or high frequency foci on the transmural surface at the site of the papillary muscle that was not seen in Controls. In the CHF model, a substrate is developed such that the papillary muscle may support the stability of VF drivers that are characterized by stable, high DF areas.

Acknowledgement

The authors would like to thank Changyu Shen, PhD, and Hongbo Lin for their help with the statistical analysis.

Author Contributions

Thomas Everett was responsible for the concept and design of the experiments, collection of data, performed the data analysis and interpretation, and drafted the manuscript.

George Hulley and Roger Chang were trainees who performed data analysis and interpretation.

Ken Lee assisted in the concept and design of the experiments and collected data.

Emily Wilson assisted in the concept and design of the experiments and collected data.

Jeffrey Olgin was responsible for the concept and design of the experiments, interpretation of the data, and generation of the manuscript.

References

1. Everett THt, Olgin JE. Ventricular arrhythmia in structurally remodeled hearts and potential role of myocardial fibrosis. In: Dudley SC, Sovari AA, Kocherile AG, eds. *Ventricular Arrhythmia From Principles to Patients*. New York: Nova Science Publishers, Inc.; 2013:37-50.

2. Anderson ME, Hodgson-Zingman DM. Ventricular Tachycardia in Patients with Heart Failure. In: Zipes DP, Jalife J, eds. *Cardiac Electrophysiology From Cell to Bedside*. 5 ed. Philadelphia, PA: Saunders Elsevier; 2009:707 - 716.

3. Holzem KM, Efimov IR. Arrhythmogenic remodelling of activation and repolarization in the failing human heart. *Europace.* 2012;14 Suppl 5:v50-v57.

4. Choi BR, Liu T, Salama G. The distribution of refractory periods influences the dynamics of ventricular fibrillation. *Circ Res.* 2001;88(5):E49-58.

5. Laurita KR, Girouard SD, Rosenbaum DS. Modulation of ventricular repolarization by a premature stimulus. Role of epicardial dispersion of repolarization kinetics demonstrated by optical mapping of the intact guinea pig heart. *Circ Res.* 1996;79(3):493-503.

6. Akar FG, Rosenbaum DS. Transmural electrophysiological heterogeneities underlying arrhythmogenesis in heart failure. *Circ Res.* 2003;93(7):638-645.

7. Poelzing S, Akar FG, Baron E, Rosenbaum DS. Heterogeneous connexin43 expression produces electrophysiological heterogeneities across ventricular wall. *Am J Physiol Heart Circ Physiol.* 2004;286(5):H2001-2009.

8. Yan GX, Shimizu W, Antzelevitch C. Characteristics and distribution of M cells in arterially perfused canine left ventricular wedge preparations. *Circulation.* 1998;98(18):1921-1927.

9. Nattel S, Antzelevitch C, Noble D. Resolving the M-cell debate: why and how. *Heart Rhythm.* 2011;8(8):1293-1295.

10. Kim YH, Xie F, Yashima M, et al. Role of papillary muscle in the generation and maintenance of reentry during ventricular tachycardia and fibrillation in isolated swine right ventricle. *Circulation.* 1999;100(13):1450-1459.

11. Pak HN, Kim YH, Lim HE, Chou CC, Miyauchi Y, Fang YH, Sun K, Hwang C, Chen PS. Role of the posterior papillary muscle and purkinje potentials in the mechanism of ventricular fibrillation in open chest dogs and Swine: effects of catheter ablation. *J Cardiovasc Electrophysiol.* 2006;17(7):777-783.

12. Everett THt, Wilson EE, Foreman S, Olgin JE. Mechanisms of ventricular fibrillation in canine models of congestive heart failure and ischemia assessed by in vivo noncontact mapping. *Circulation.* 2005;112(11):1532-1541.

13. Wu J, Biermann M, Rubart M, Zipes DP. Cytochalasin D as excitation-contraction uncoupler for optically mapping action potentials in wedges of ventricular myocardium. *J Cardiovasc Electrophysiol.* 1998;9(12):1336-1347.

14. Salama G, Choi BR, Azour G, Lavasani M, Tumbev V, Salzberg BM, Patrick MJ, Ernst LA, Waggoner AS. Properties of new, long-wavelength, voltage-sensitive dyes in the heart. *J Membr Biol.* 2005;208(2):125-140.

15. Everett THt, Kok LC, Vaughn RH, Moorman JR, Haines DE. Frequency domain algorithm for quantifying atrial fibrillation organization to increase defibrillation efficacy. *IEEE Trans Biomed Eng.* 2001;48(9):969-978.

16. Nguyen DT, Ding C, Wilson E, Marcus GM, Olgin JE. Pirfenidone mitigates left ventricular fibrosis and dysfunction after myocardial infarction and reduces arrhythmias. *Heart Rhythm.* 2010;7(10):1438-1445.

17. Liu DW, Antzelevitch C. Characteristics of the delayed rectifier current (IKr and IKs) in canine ventricular epicardial, midmyocardial, and endocardial myocytes. A weaker IKs contributes to the longer action potential of the M cell. *Circ Res.* 1995;76(3):351-365.

18. Sicouri S, Antzelevitch C. A subpopulation of cells with unique electrophysiological properties in the deep subepicardium of the canine ventricle. The M cell. *Circ Res.* 1991;68(6):1729-1741.

19. Poelzing S. Are electrophysiologically distinct M-cells a characteristic of the wedge preparation? *Heart Rhythm.* 2009;6(7):1035-1037.

20. Dean JW, Lab MJ. Regional changes in ventricular excitability during load manipulation of the in situ pig heart. *The Journal of physiology.* 1990;429:387-400.

21. Burton FL, Cobbe SM. Effect of sustained stretch on dispersion of ventricular fibrillation intervals in normal rabbit hearts. *Cardiovasc Res.* 1998;39(2):351-359.

22. Efimov IR, Sidorov V, Cheng Y, Wollenzier B. Evidence of three-dimensional scroll waves with ribbon-shaped filament as a mechanism of ventricular tachycardia in the isolated rabbit heart. *J Cardiovasc Electrophysiol.* 1999;10(11):1452-1462.

23. Myles RC, Burton FL, Cobbe SM, Smith GL. The link between repolarisation alternans and ventricular arrhythmia: does the cellular phenomenon extend to the clinical problem? *J Mol Cell Cardiol.* 2008;45(1):1-10.

24. Laurita KR, Wilson LD, Rosenbaum DS. *Cardiac alternans as a pathophysiologic mechanism of arrhythmias*. 5 ed. Philadelphia, PA: Saunders Elsevier; 2009.

25. Wilson LD, Jeyaraj D, Wan X, Hoeker GS, Said TH, Gittinger M, Laurita KR, Rosenbaum DS. Heart failure enhances susceptibility to arrhythmogenic cardiac alternans. *Heart Rhythm.* 2009;6(2):251-259.

26. Huang J, Rogers JM, Killingsworth CR, Walcott GP, KenKnight BH, Smith WM, Ideker RE. Improvement of defibrillation efficacy and quantification of activation patterns during ventricular fibrillation in a canine heart failure model. *Circulation.* 2001;103(10):1473-1478.

27. Moreno J, Zaitsev AV, Warren M, Berenfeld O, Kalifa J, Lucca E, Mironov S, Guha P, Jalife J. Effect of remodelling, stretch and ischaemia on ventricular fibrillation frequency and dynamics in a heart failure model. *Cardiovasc Res.* 2005;65(1):158-166.

28. Berenfeld O, Pertsov AM. Dynamics of intramural scroll waves in three-dimensional continuous myocardium with rotational anisotropy. *J Theor Biol.* 1999;199(4):383-394.

29. Li L, Jin Q, Huang J, Cheng KA, Ideker RE. Intramural foci during long duration fibrillation in the pig ventricle. *Circ Res.* 2008;102(10):1256-1264.

30. Valderrabano M, Lee MH, Ohara T, Lai AC, Fishbein MC, Lin SF, Karagueuzian HS, Chen PS. Dynamics of intramural and transmural reentry during ventricular fibrillation in isolated swine ventricles. *Circ Res.* 2001;88(8):839-848.

31. Glukhov AV, Fedorov VV, Lou Q, Ravikumar VK, Kalish PW, Schuessler RB, Moazami N, Efimov IR. Transmural dispersion of repolarization in failing and nonfailing human ventricle. *Circ Res.* 2010;106(5):981-991.

32. Voss F, Opthof T, Marker J, Bauer A, Katus HA, Becker R. There is no transmural heterogeneity in an index of action potential duration in the canine left ventricle. *Heart Rhythm.* 2009;6(7):1028-1034.

33. Biermann M, Rubart M, Moreno A, Wu J, Josiah-Durant A, Zipes DP. Differential effects of cytochalasin D and 2,3 butanedione monoxime on isometric twitch force and transmembrane action potential in isolated ventricular muscle: implications for optical measurements of cardiac repolarization. *J Cardiovasc Electrophysiol.* 1998;9(12):1348-1357.

34. Lou Q, Li W, Efimov IR. The role of dynamic instability and wavelength in arrhythmia maintenance as revealed by panoramic imaging with blebbistatin vs. 2,3-butanedione monoxime. *Am J Physiol Heart Circ Physiol.* 2012;302(1):H262-269.

Figure Legends

Figure 1. Summary data comparing conduction velocity (CV) and phase anisotropy metrics between models (Control and CHF) for each pacing cycle length on each surface. Each data point represents the combined data from all pacing sites.

Figure 2. (A) Summary data for the mean APD_{80} (top panels) and APD_{80} variability (bottom panels), comparing the mapped surfaces for each model of Control (left panels) and CHF (right panels). Each data point represents the combined data from all pacing sites.
(B) Calculation of the APD_{80} gradient at each pacing cycle length for each surface of the CHF model. (C) APD_{80} map from a CHF transmural surface at a pacing rate of 400 ms. Representative examples of optical action potentials are also shown.

Figure 3. (A) Percentage of APD_{80} alternans that were observed on each surface for each group for Control and CHF correlated to VF vulnerability. (B) An example signal from the transmural surface in the CHF group showing alternating APD_{80}. (C) Percentage of VF induced with an extra stimulus (S2) on each surface for Control and CHF.

Figure 4. Activation maps from an S2 in which VF was initiated in both CHF and Control examples on the epicardial surface. Pacing is from the lateral side in both examples. The arrows indicate the direction of propagation.

Figure 5. Conduction velocity and phase metrics correlated to VF inducibility. Calculating phase was used to quantify conduction anisotropy. Panel A – p50; Panel B – p95-p5; Panel C – (p95-p5)/p50; along with mean conduction velocity – Panel D for each mapped surface in Control and CHF.

Figure 6. APD_{80} variability as calculated by the difference between the 95^{th} percentile and the 5^{th} percentile correlated to VF vulnerability on each mapped surface for Control and CHF.

Figure 7. Activation maps of the different types of ventricular fibrillation mechanisms that were observed with optical mapping. The arrows indicate the direction of propagation.

Figure 8. (A) Examples of static DF maps from the Control group (right panels) and the CHF group (left panels). All examples from each surface are from the same dog for that group. In the Control example, multiple wavefronts were seen on the epicardial surface, and one broad wavefront on the endocardial and transmural surfaces. In the CHF example, a spiral wave was seen on the transmural surface with focal activity on the endocardial surface, and one broad wavefront on the epicardium. The spiral wave on the transmural surface correlated to the highest DF that was seen in this preparation. **(**B) APD_{80} versus the top 10% of DFs and the bottom 10% of DFs for each surface in the CHF model. (C) APD_{80} versus the top 10% of DFs and the bottom 10% of DFs for the epicardial surface for individual dogs in the CHF group.

	VF Activation Patterns			Stable High DF		
Dog	Epicardial	Endocardial	Transmural	Epicardial	Endocardial	Transmural
Control Dog 1	broad wavefront	spiral wave				
Control Dog 2	broad wavefront	multiple wave				
Control Dog 3	multiple wave	broad wavefront				
Control Dog 4	focal	spiral wave	focal	X		X
Control Dog 5	multiple wave	broad wavefront	broad wavefront			
Control Dog 6			focal			X
Control Dog 7	multiple wave					
Control Dog 8	multiple wave	multiple wave	focal			
Control Dog 9	broad wavefront					
Control Dog 10	focal			X		
Control Dog 11	broad wavefront	broad wavefront				
CHF Dog 1	spiral wave		spiral wave	X		X
CHF Dog 2	broad wavefront					
CHF Dog 3	multiple wave	spiral wave	focal		X	X
CHF Dog 4	focal	multiple wave	focal	X		X
CHF Dog 5	broad wavefront	focal	spiral wave		X	X
CHF Dog 6		spiral wave			X	
CHF Dog 7	multiple wave	multiple wave	focal			X

Table 1 - VF mechanism as determined by the VF activation patterns, and location of stable, high DF areas.

Figure 1

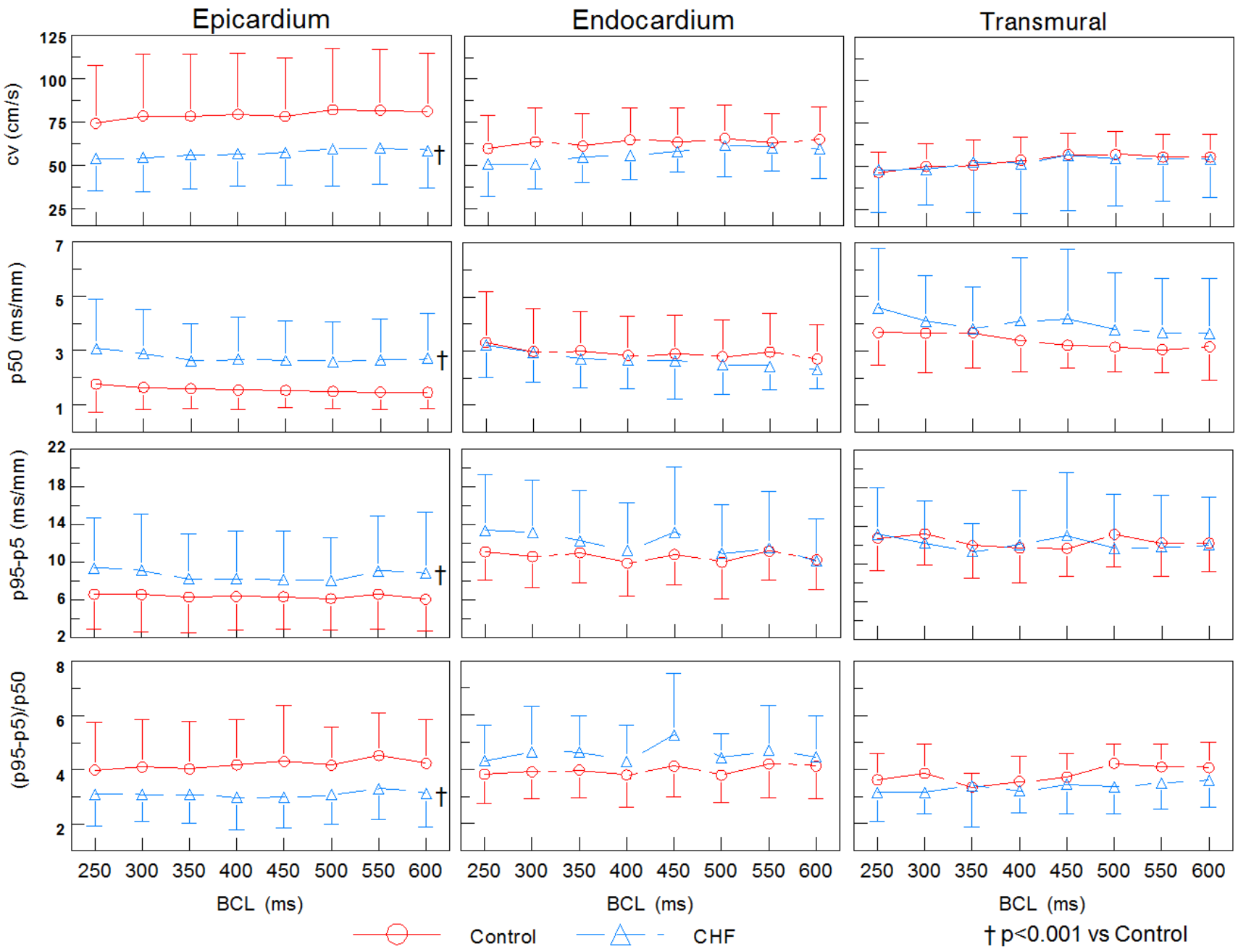
Epicardium
Endocardium
Transmural
cv (cm/s)
p50 (ms/mm)
p95-p5 (ms/mm)
(p95-p5)/p50
†
BCL (ms)
Control
CHF
† p<0.001 vs Control

Figure 2

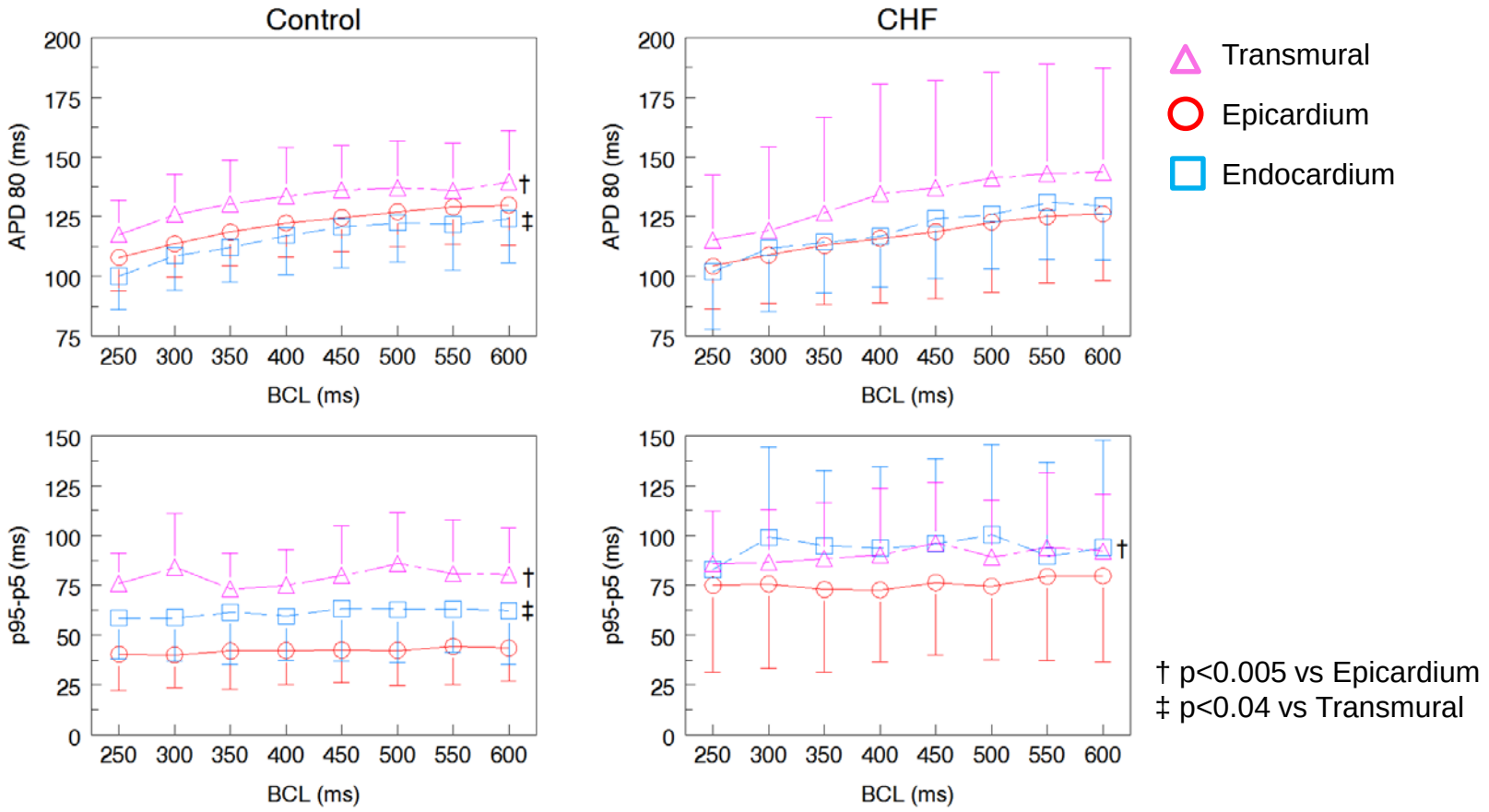
A.
Control
CHF
APD 80 (ms)
p95-p5 (ms)
BCL (ms)
Transmural
Epicardium
Endocardium
† p<0.005 vs Epicardium
‡ p<0.04 vs Transmural

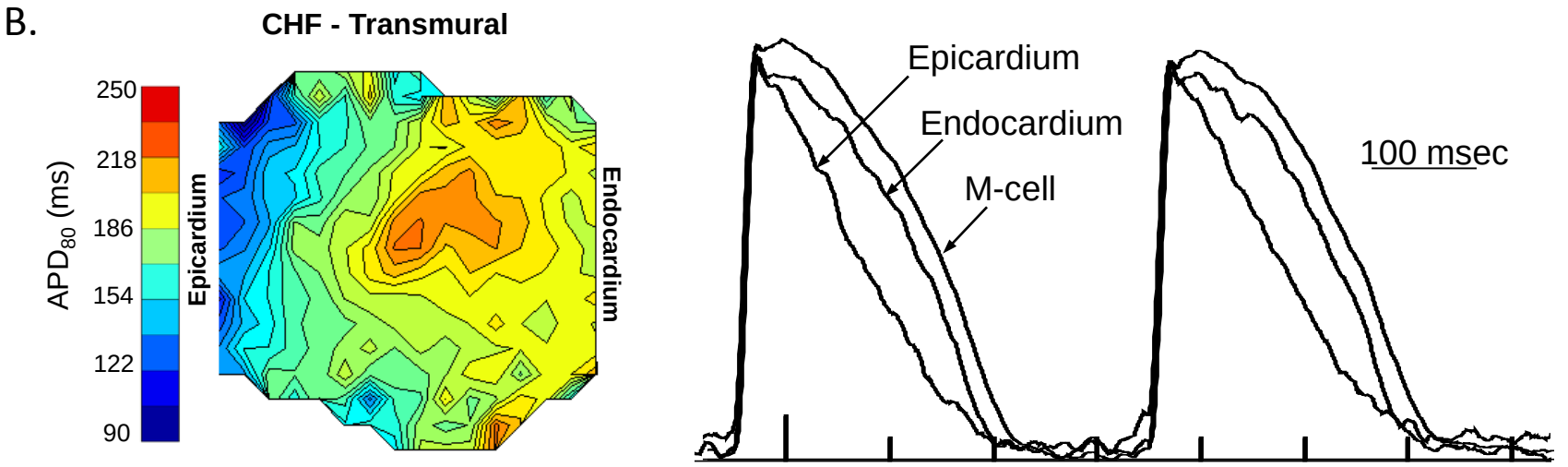
B.
CHF - Transmural
APD80 (ms)
Epicardium
Endocardium
Epicardium
Endocardium
M-cell
100 msec

Figure 3

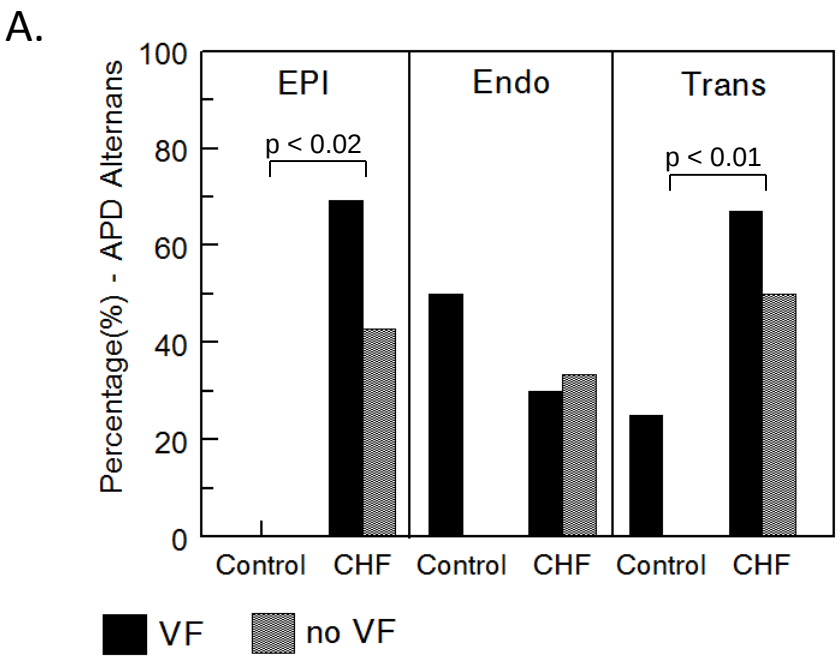
A.
Percentage(%) - APD Alternans
100
80
60
40
20
0
EPI
Endo
Trans
p < 0.02
p < 0.01
Control
CHF
Control
CHF
Control
CHF
VF
no VF

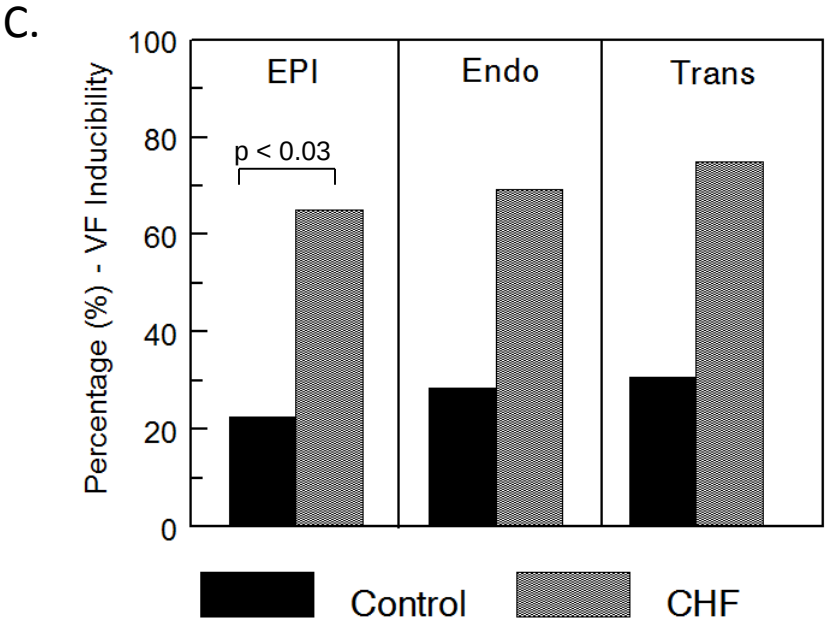
C.
Percentage (%) - VF Inducibility
100
80
60
40
20
0
EPI
Endo
Trans
p < 0.03
Control
CHF

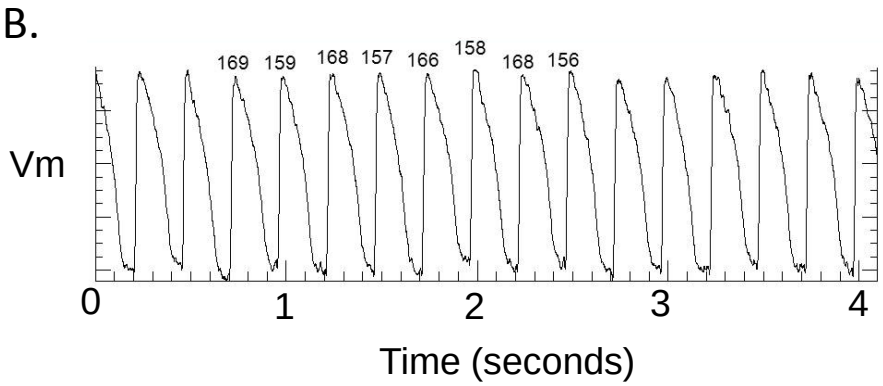
B.
Vm
169
159
168
157
166
158
168
156
0
1
2
3
4
Time (seconds)

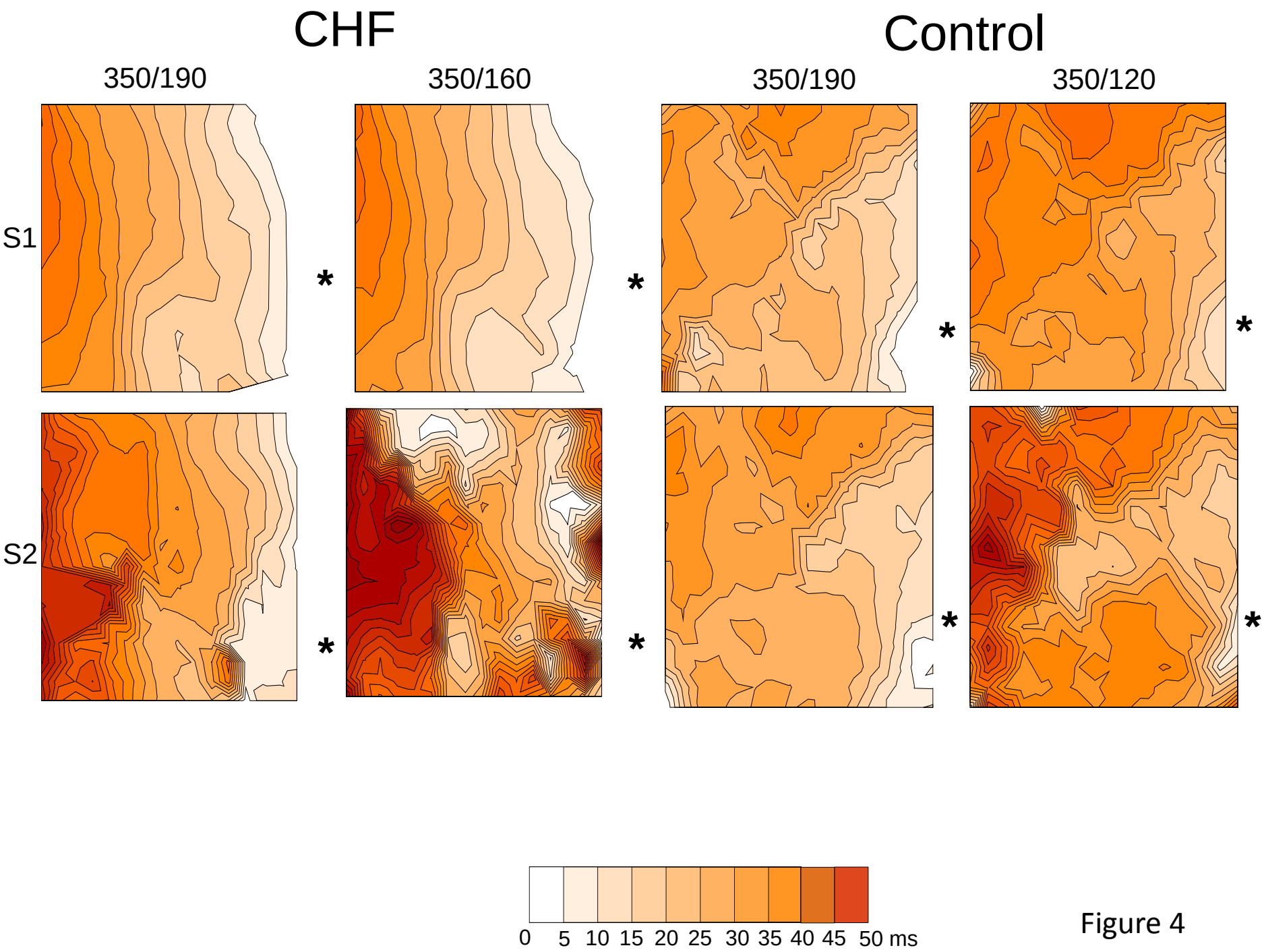
CHF
Control
350/190
350/160
350/190
350/120
S1
S2
*
*
*
*
*
*
*
*
0 5 10 15 20 25 30 35 40 45 50 ms

Figure 4

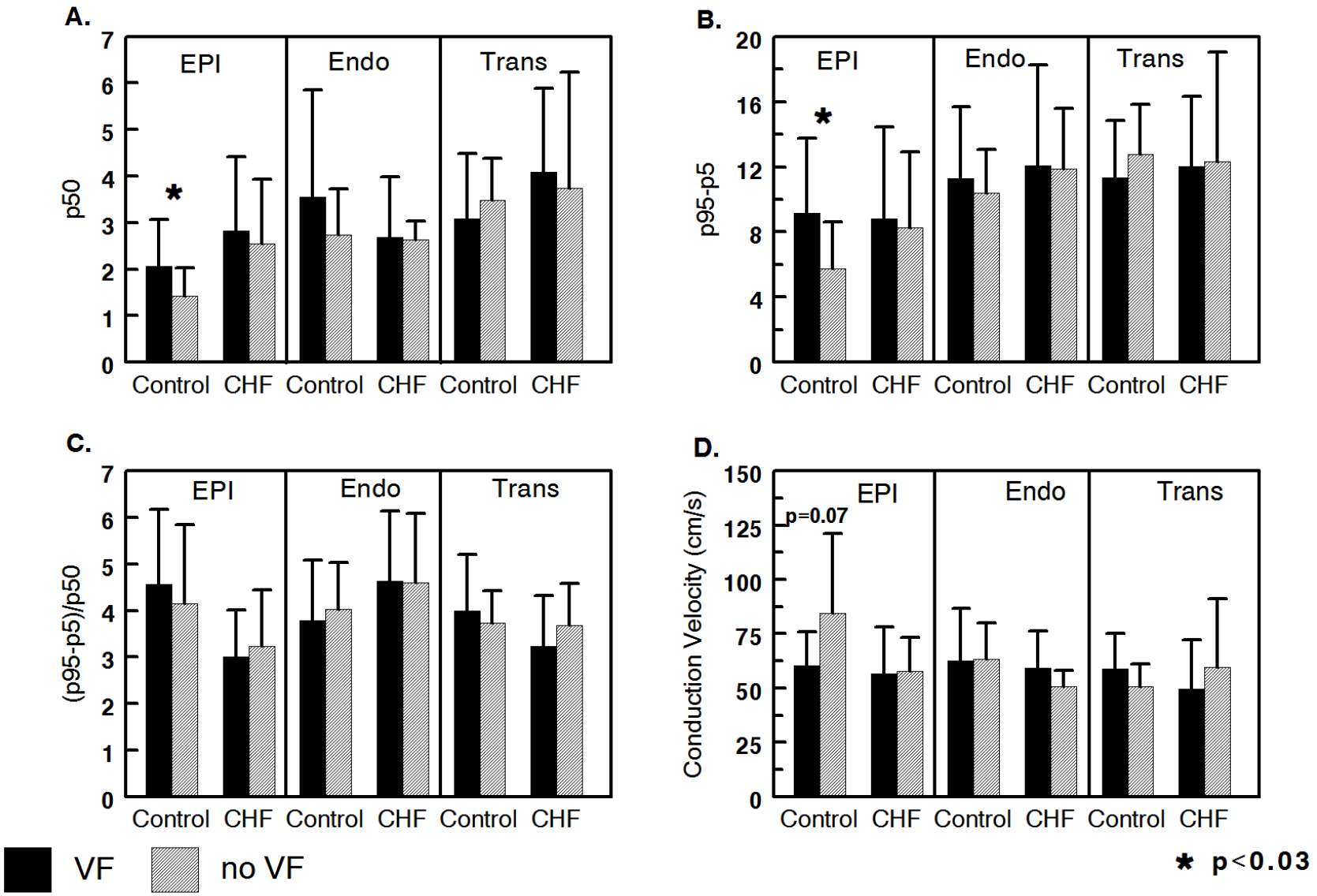
A.
p50
EPI
Endo
Trans
Control
CHF
B.
p95-p5
C.
(p95-p5)/p50
D.
Conduction Velocity (cm/s)
p=0.07
VF
no VF
* p<0.03

Figure 5

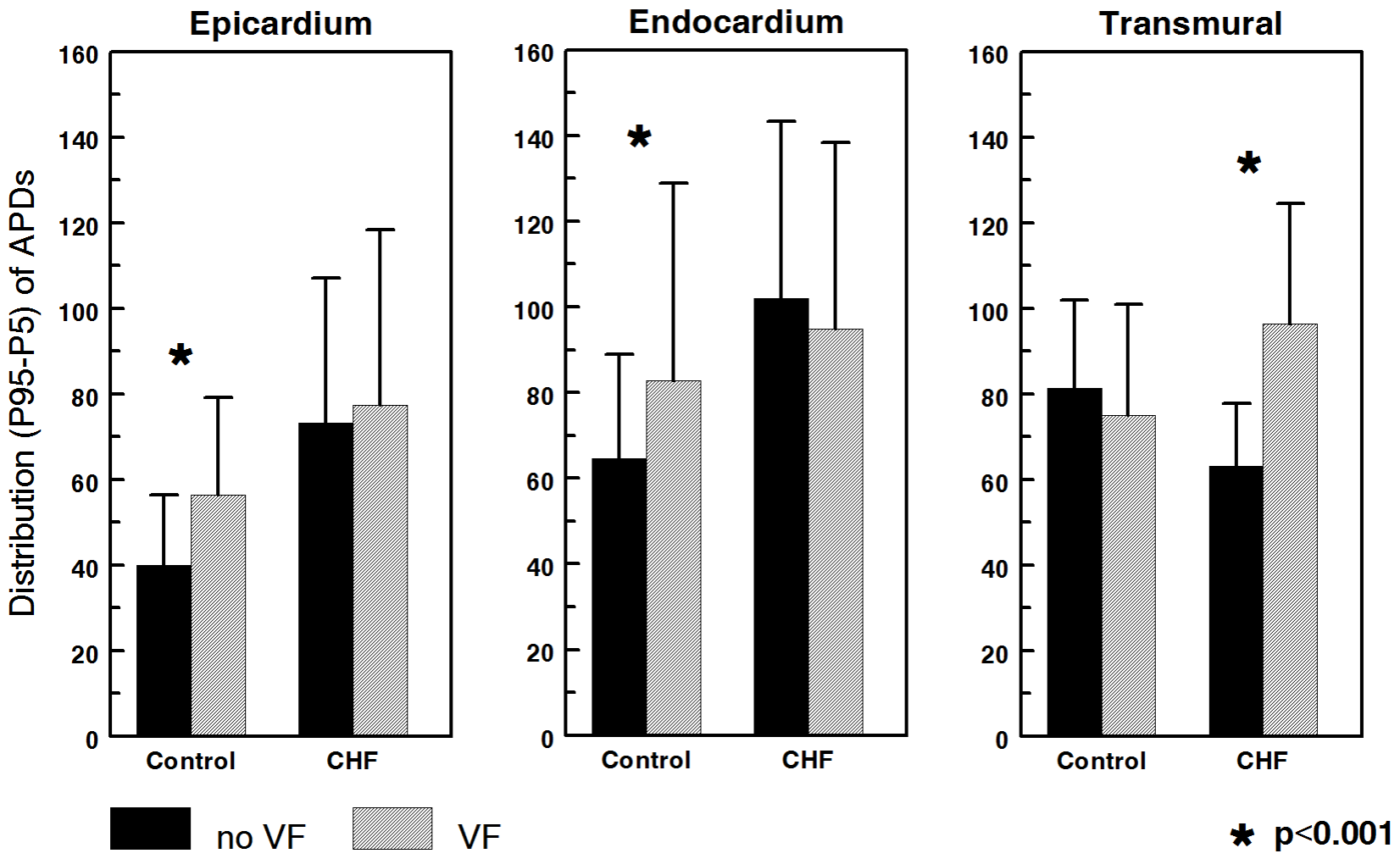
Epicardium
Endocardium
Transmural
Distribution (P95-P5) of APDs
160
140
120
100
80
60
40
20
0
Control
CHF
*
no VF
VF
* p<0.001

Figure 6

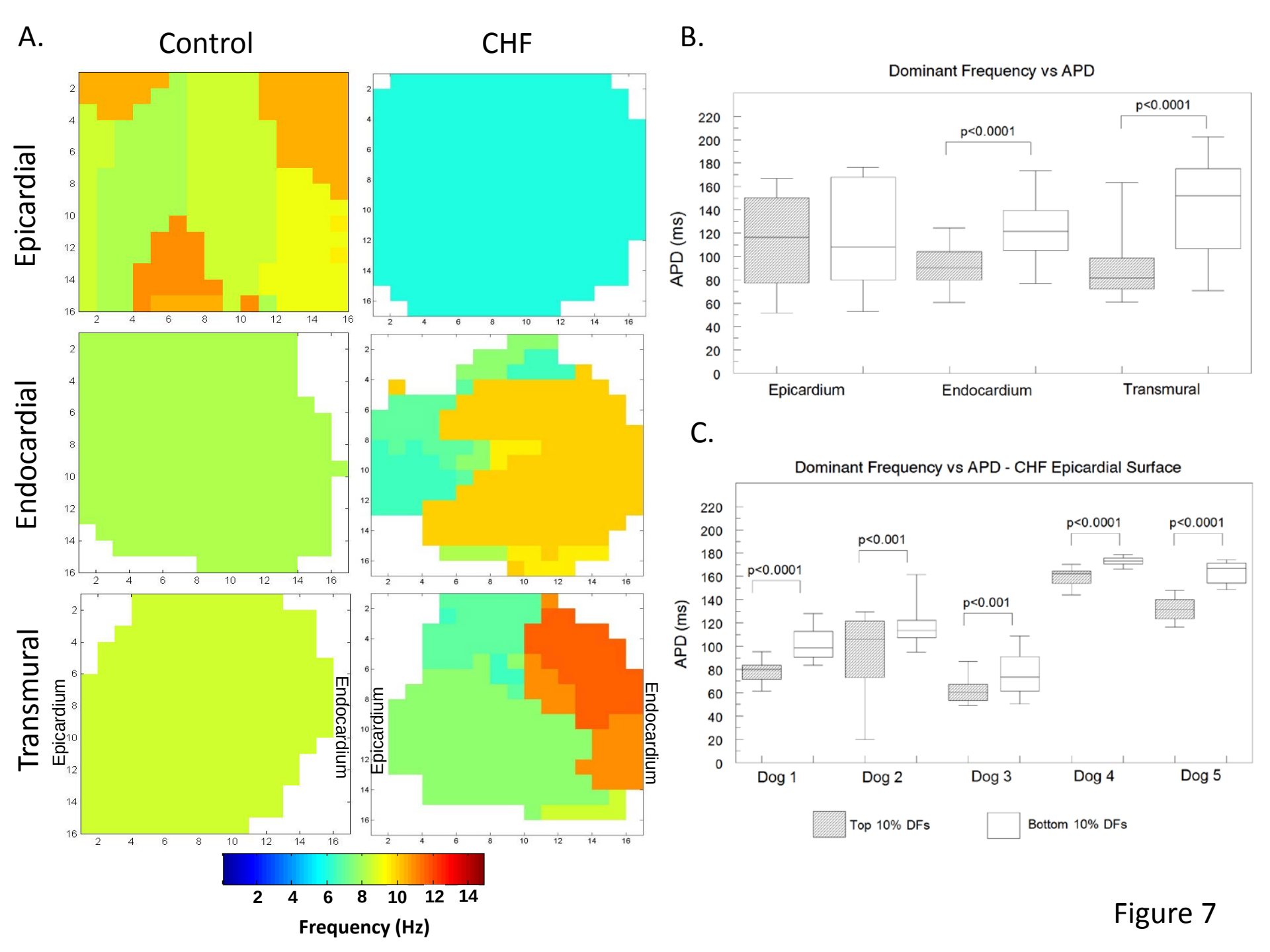
A.
Control
CHF
Epicardial
Endocardial
Transmural
Epicardium
Endocardium
Epicardium
Endocardium
2 4 6 8 10 12 14
Frequency (Hz)
B.
Dominant Frequency vs APD
APD (ms)
p<0.0001
p<0.0001
Epicardium
Endocardium
Transmural
C.
Dominant Frequency vs APD - CHF Epicardial Surface
APD (ms)
p<0.0001
p<0.001
p<0.001
p<0.0001
p<0.0001
Dog 1
Dog 2
Dog 3
Dog 4
Dog 5
Top 10% DFs
Bottom 10% DFs

Figure 7